JCI insight

TMEM16B determines cholecystokinin sensitivity of intestinal vagal afferents of nodose neurons

Runping Wang, … , Mark W. Chapleau, François M. Abboud

JCI Insight. 2019;4(5):e122058. https://doi.org/10.1172/jci.insight.122058.

Research Article | Cell biology | Metabolism

Graphical abstract

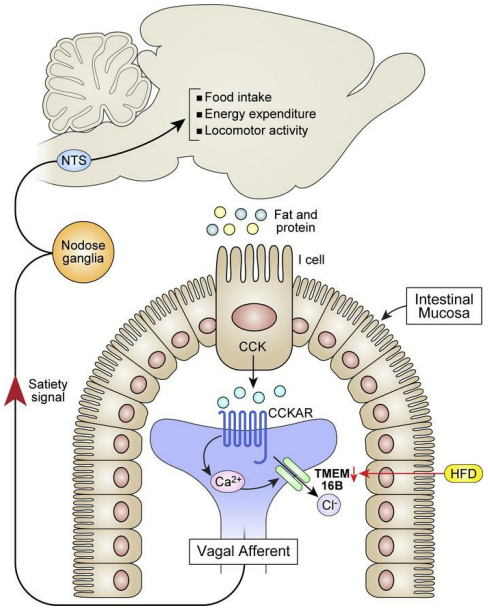

JCI insight

RESEARCH ARTICLE

TMEM16B determines cholecystokinin sensitivity of intestinal vagal afferents of nodose neurons

Runping Wang,[1,2] Yongjun Lu,[1,2] Michael Z. Cicha,[1,2] Madhu V. Singh,[1,2] Christopher J. Benson,[1,2,3,4] Christopher J. Madden,[5] Mark W. Chapleau,[1,2,3,4] and François M. Abboud[1,2,3]

[1]Department of Internal Medicine, [2]Abboud Cardiovascular Research Center, and [3]Department of Molecular Physiology and Biophysics, University of Iowa, Iowa City, Iowa, USA. [4]Veterans Affairs Medical Center, Iowa City, Iowa, USA. [5]Department of Neurological Surgery, Oregon Health & Science University, Portland, Oregon, USA.

The satiety effects and metabolic actions of cholecystokinin (CCK) have been recognized as potential therapeutic targets in obesity for decades. We identified a potentially novel Ca^{2+}-activated chloride (Cl^-) current (CaCC) that is induced by CCK in intestinal vagal afferents of nodose neurons. The CaCC subunit *Anoctamin* 2 (*Ano2*/TMEM16B) is the dominant contributor to this current. Its expression is reduced, as is CCK current activity in obese mice on a high-fat diet (HFD). Reduced expression of TMEM16B in the heterozygote KO of the channel in sensory neurons results in an obese phenotype with a loss of CCK sensitivity in intestinal nodose neurons, a loss of CCK-induced satiety, and metabolic changes, including decreased energy expenditure. The effect on energy expenditure is further supported by evidence in rats showing that CCK enhances sympathetic nerve activity and thermogenesis in brown adipose tissue, and these effects are abrogated by a HFD and vagotomy. Our findings reveal that *Ano2*/TMEM16B is a Ca^{2+}-activated chloride channel in vagal afferents of nodose neurons and a major determinant of CCK-induced satiety, body weight control, and energy expenditure, making it a potential therapeutic target in obesity.

Introduction

Obesity represents a major risk factor associated with diabetes, ischemic heart attacks, stroke, sleep apnea, and cancer (1, 2). Current pharmaceutical interventions are ineffective at maintaining weight loss and cause multiple side effects (3). Impaired satiety signaling in the gastrointestinal tract becomes important in initiating weight gain and obesity (4). Gut peptide hormones released in response to food intake and related satiety signals conducted by vagal afferent neurons have become potential targets for future therapeutic intervention (5, 6).

Gastrointestinal vagal afferents are important in controlling satiety and food intake (7, 8). Chemical contents of food are detected by specialized cells in the gut that secrete peptide hormones, such as cholecystokinin (CCK), glucagon like peptide-1 (GLP1), and peptide tyrosine tyrosine (PYY). Obesity involves imbalanced vagal afferent anorexigenic and orexigenic signals (8). Sensitivity to anorexigenic vagal signals such as mechanical distention, leptin, PYY, GLP-1, and CCK is reduced. CCK is a major paracrine satiety hormone secreted after intake of fat and protein (5, 7, 9). Its suppressive effect on food intake is reduced in obesity (10, 11). Administration of CCK decreases meal size and increases meal duration (5, 7, 12, 13). Conversely, administration of a CCK1 (CCKA) receptor antagonist decreases feelings of fullness and increases meal size in humans (5, 14). Activation of intestinal vagal afferents by CCK through CCK1 (CCKA) receptor transduces the short-term satiety signal to the nucleus tractus solitarius (NTS) and hypothalamus to terminate food intake and, in addition, increases metabolism and limits weight gain (15, 16). Recordings from vagal afferents indicate that both spontaneous and CCK-induced nerve activity is reduced in obese mice on a high-fat diet (HFD) (17). There is a decrease in neuronal excitability and the number of neurons responding to CCK, but the ion channels involved in the activation of these neurons have not been defined.

CCK activates G protein coupled CCK1 (CCKA) receptors, leading to activation of phospholipase C/diacylglycerol/inositol-1,4,5-trisphosphate (PLC/DAG/IP3) signaling, an increase in intracellular Ca^{2+}, and activation of protein kinase C (PKC) (18–22). In HFD-induced obesity, CCK1 (CCKA) receptor

Conflict of interest: All authors declare that no conflict of interest exists.

Submitted: May 7, 2018
Accepted: January 17, 2019
Published: March 7, 2019

Reference information:
JCI Insight. 2019;4(5):e122058.
https://doi.org/10.1172/jci.insight.122058.

expression and CCK levels are both increased (23–25), but paradoxically, the CCK-induced response is decreased (10, 11, 17). We investigated whether defects in ion channels induced by CCK in vagal afferent neurons contribute to this paradox.

Multiple K^+ channels, transient receptor potential (TRP) channels, and cholinergic nicotinic receptors (nAchR) in adipose tissue and in the central as well as the peripheral sensory nervous system are involved in obesity (26). Increased TWIK-related acid-sensitive K^+ (TASK) channel–mediated current contributes to HFD-induced vagal afferent dysfunction (27). Ion channels involved in CCK-induced responses include L-type voltage–dependent Ca^{2+} channels and TRP channels that contribute to the neuronal Ca^{2+} influx elicited by CCK (21, 28–30). ATP-sensitive potassium channel (K_{ATP}) and A-type K channels may also be involved in responses to CCK (31, 32).

Our goals were to (a) define the ionic current induced by CCK in nodose neurons; (b) determine whether the channel expression and its activity are reduced in intestinal nodose neurons of mice fed HFD; and (c) characterize the phenotype in the heterozygote KO of the channel.

Here, we report a calcium-activated Cl^- current (CaCC) induced by CCK in intestinal nodose neurons. *Ano2*/TMEM16B (*Anoctamin-2*/*Transmembrane member 16B*) is the dominant subunit of the channel conducting this CaCC. We also investigated whether the expression of this channel is reduced in obese mice fed a HFD. Finally, we knocked out 1 allele of the *Ano2* gene by crossing the floxed $Ano2^{fl/fl}$ mice with mice expressing Cre in nodose neurons driven by $Na_v1.8$ promoter and measured weight gain, CCK responses, and other phenotypic characteristics of the heterozygote mice.

Results

CCK induces a Cl– current in nodose ganglia neurons

CCK-8, a major form of CCK in the proximal intestine (33), has been reported to induce activation of several cation channels in different tissues (21, 28–31). To test whether nodose neurons respond to CCK, we cultured the dissociated nodose ganglia (NG) neurons from mice and recorded the CCK-induced current using whole-cell patch-clamp. With a symmetrical concentration of Cl^- on both sides of the membrane, extracellular application of 10 nM CCK-8 induced a large and sustained inward current (32.5 ± 6.1 pA/pF, $n = 15$) that recovered after removing CCK (Figure 1A). The induction of the current by CCK was dose dependent, with a significant current induced by a CCK concentration as low as 0.01 nM (Figure 1A).

We replaced intracellular Cl^- ($[Cl^-]_i$) in the pipette solution with aspartate and reduced the $[Cl^-]_i$ from 133 mM to 4 mM. The CCK-induced inward current was eliminated (Figure 1B), indicating that the current is likely caused by anion efflux of Cl^-. In confirmation, we measured the current-voltage relationship (I-V curve) and the reversal potential by lowering the extracellular Cl^- ($[Cl^-]_o$) concentration from 133 mM to 68 mM and 4 mM. The reversal potential of the CCK-induced current was ~ 0 mV, with equal concentration of Cl^- on both sides of the membrane, and gradually shifted to more positive voltage with 68 mM and 4 mM of $[Cl^-]_o$. The plot of the reversal potential showed a linear relationship with the logarithmic concentration of $[Cl^-]_o$, which is consistent with the properties of Cl^- channels (Figure 1C).

The CCK-induced Cl^- current is Ca^{2+} dependent. We tested the Ca^{2+} dependence of this CCK-induced Cl^- current (22, 34). $[Ca^{2+}]_i$ was recorded using calcium imaging by loading nodose neurons with Fluo-4/AM. Application of increasing concentrations of CCK-8 from 0.1 nM to 1000 nM induced a dose-dependent increase in $[Ca^{2+}]_i$ with an EC_{50} of 1.2 ± 0.5 nM and a plateau level at 10 nM of CCK-8 (Figure 1D), which is consistent with previous reports (35, 36). Moreover, buffering $[Ca^{2+}]_i$ with 10 mM of the fast Ca^{2+} chelator BAPTA completely eliminated the CCK-8 induced current (Figure 1E), confirming its Ca^{2+} dependence.

TMEM16B is the major subunit of the CCK-induced Cl– channel in nodose neurons

Two subunits of the Ca^{2+}-activated Cl^- channel (CaCC) family have been cloned, TMEM16A (*Ano1*) and TMEM16B (*Ano2*), with TMEM16A showing a 10-fold higher sensitivity to $[Ca^{2+}]_i$ than TMEM16B (37). TMEM16A is activated by $[Ca^{2+}]_i$ as low as 0.1 μM, whereas TMEM16B activation requires concentrations higher than 1 μM (38, 39). To determine the relative sensitivity to $[Ca^{2+}]_i$ in nodose neurons, we used excised inside-out patches exposed to a series of intracellular Ca^{2+} concentration buffered by 1 mM EGTA and found that the Cl^- channel responded only to $[Ca^{2+}]_i$ higher than 1 μM (Figure 2A), supporting the dependence of CCK-8–induced CaCC on TMEM16B rather than TMEM16A. We also found that the specific TMEM16A inhibitor $T16A_{inh\text{-}A01}$ (T16A) did not attenuate the CCK-8–induced response (Figure 2B).

Niflumic acid (NFA) is a more potent CaCC inhibitor of TMEM16A, with an inhibition of ~90% of the TMEM16A current with 100 μM NFA (40) and only ~60% inhibition of the TMEM16B current at 300 μM (41). Our results confirm the necessity of the higher concentration of NFA (300 μM) in order to cause significant inhibition of 61.7% of the CCK-induced current and further support the dominance of TMEM16B in this response (Figure 2C).

Effect of shRNA on neuronal TMEM16 expression and CCK-induced current. To more directly determine the dominance of TMEM16B in this response, we transduced nodose neurons with lentivirus carrying shRNA against TMEM16B and control virus with scrambled RNA. The vector also carried a puromycin-resistant gene, and nodose neurons were exposed 2 days later to 3 μg/ml of puromycin to selectively favor the survival of transduced neurons that would be resistant to puromycin. Control neurons transduced with scrambled shRNA sequences presented robust CCK-induced currents, whereas neurons transduced with TMEM16B shRNA showed a 79.8% decrease in CCK-induced current density (Figure 2D). The mRNA expression of TMEM16B measured by single cell quantitative PCR (qPCR) in individual neurons 2 days after transduction was reduced significantly in neurons transduced with shRNA compared with neurons transduced with scrambled sequences ($P < 0.05$; Figure 2E).

HFD suppresses CCK-8–induced CaCC and expression of TMEM16B in nodose neurons

CCK-induced satiety signaling and vagal afferent excitability are reduced with HFD-induced obesity, despite normal or high levels of CCK (17, 24, 25, 42, 43). We investigated whether a defect in CCK receptors and/or the CaCC channel account for this CCK insensitivity in HFD-induced obesity. C57BL/6 mice were fed a HFD with 60% of calories from fat for 12–14 weeks, and control mice were fed normal chow with 18% of calories from fat. Mice fed a HFD had a 31.4% greater increase in body weight compared with mice fed regular chow (Figure 3A). The age of mice in these 2 groups was similar (21.0 ± 0.5 weeks in chow-fed mice and 20.6 ± 0.4 weeks in HFD mice). The HFD diet was started at 8 weeks of age.

Expression of CCK receptors and responses of $[Ca^{2+}]_i$ to CCK are preserved in nodose neurons of mice on HFD. The level of CCK1 (CCKA) receptor mRNA in NG from mice fed a HFD was 48% higher than in mice fed regular chow ($P < 0.05$), and the mRNA level of CCK2 (CCKB) receptor was similar in the 2 groups (Figure 3B). The results are consistent with previous reports showing that CCK receptors are not decreased and may be increased in HFD-induced obesity (23).

Since an increase in $[Ca^{2+}]_i$ is required for CCK-induced activation of the CaCC channel, we tested whether the CCK-induced Ca^{2+} signal is reduced in nodose neurons of obese mice fed a HFD. We found that the $\Delta[Ca^{2+}]_i$ in response to CCK over a wide dose range was not significantly different in nodose neurons from mice fed a HFD vs. regular chow (Figure 3F), indicating that CCK insensitivity is caused by events downstream of the CCK receptor and Ca^{2+} signal.

Expression of TMEM16 subunits is reduced in NG of mice on a HFD. In NG of obese mice on a HFD, the mRNA levels of CaCC subunit TMEM16A/*Ano1* were decreased by 40%, and those of TMEM16B/*Ano2* subunit were decreased by 71% compared with control (Figure 3C). Immunostaining using specific antibodies also showed a marked reduction of both TMEM16A and TMEM16B protein levels in NG in HFD-fed mice compared with control mice. The reduction is more obvious in Z-section and 3-dimensional images (Figure 3, D and E).

Please refer to Supplemental Figure 4 (supplemental material available online with this article; https://doi.org/10.1172/jci.insight.122058DS1) for additional fluorescence images from different NG slices that confirm the reduction in TMEM16A and -B on HFD while the DAPI nuclear staining is preserved. Supplemental Figure 5A demonstrates fluorescent nodose neurons in culture showing DAPI nuclear staining (blue), neurofilament light chain (NFL, green), *Ano2*/TMEM16B (red), and their merged image. In Supplemental Figure 5B, the localization of TMEM16B to the neuronal cytoplasmic membrane is evident.

CCK-induced CaCC current is reduced in intestinal nodose neurons of mice on HFD. We then investigated whether the reduction of TMEM16B mRNA and protein in obese mice fed a HFD leads to a decrease in the CCK-induced current, specifically in intestinal nodose neurons. We labeled nodose neurons innervating the proximal intestine by injecting 1,1'-Dioctadecyl-3,3,3′,3'-tetramethylindocarbocyanine perchlorate (DiI) into the wall of the jejunum and duodenum 2 weeks before culturing the neurons. Only neurons with strong red fluorescence were used for recording. The CCK-induced CaCC current was defined as the magnitude of current inhibited by 300 μM NFA. This current was markedly reduced by 61% in neurons from mice on a HFD compared with neurons from mice on regular chow (Figure 3G). On the other hand, in another Cl^-

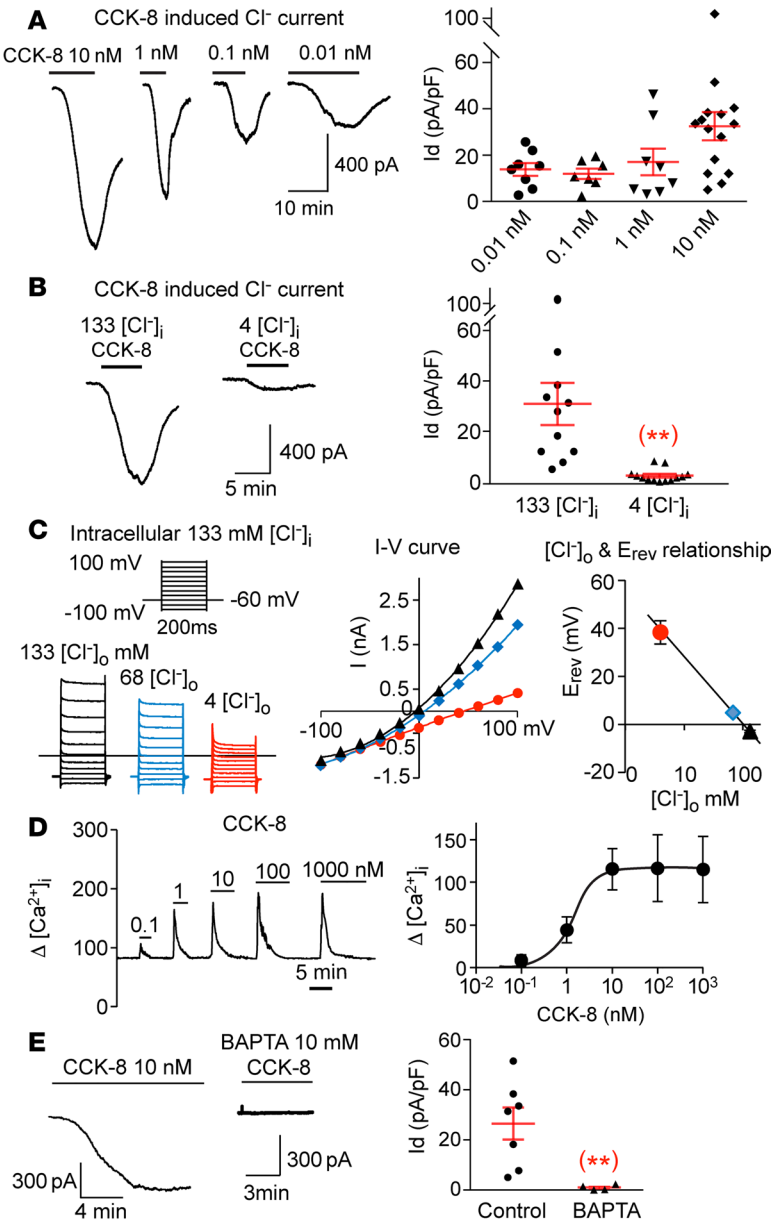

Figure 1. CCK-8 induces a Cl^- current in nodose neurons. (**A**) CCK-8 dose-dependently induces a large inward current with peak values at 32.5 ± 6.1, 17.1 ± 5.8, 12.0 ± 2.4, and 13.9 ± 2.8 pA/pF for 10, 1, 0.1 and 0.01 nM of CCK-8, respectively (n = 7–15 neurons at each dose level from a total of 10 ganglia of 5 mice). (**B**) The CCK-8 (10 nM) induced current in individual neuron is reduced significantly (**P < 0.01) from 30.9 ± 8.3 (n = 11) to 2.5 ± 0.7 pA/pF (n = 13) (obtained from 6 ganglia of 3 mice), by reducing $[Cl^-]_i$ from 133 to 4 mM. (**C**) The reversal potentials of CCK-8–induced currents obtained with 133 mM $[Cl^-]_i$ shows a linear relationship with logarithmic concentration of $[Cl^-]_o$, which decreases from133 mM (black) to 68 mM (blue) and 4 mM (red). The corresponding reversal potentials are –3.0 ± 0.4, 4.9 ± 0.3, and 38.3 ± 4.9 mV (n = 3 neurons from 2 ganglia of 1 mouse). (**D**) CCK-8 induced a rapid dose-dependent increase in $[Ca^{2+}]_i$ with a maximal response reached with 10 nM and an EC50 at 1.2 ± 0.5 nM (n = 17–34 neurons from 6 ganglia of 3 mice). (**E**) The CCK-induced current is eliminated (**P < 0.01) from 26.5 ± 6.4 (n = 7) to 1.0 ± 0.5 pA/pF (n = 4 neurons from 4 ganglia of 2 mice), with 10 mM of the fast Ca^{2+} chelator BAPTA in the pipette solution. Throughout, data are presented as means ± SEM, unpaired 2-tailed Student's t test (**B** and **E**). Each data point in **A**, **B**, and **E** represents an individual nodose neuron obtained from a total of 10 mice.

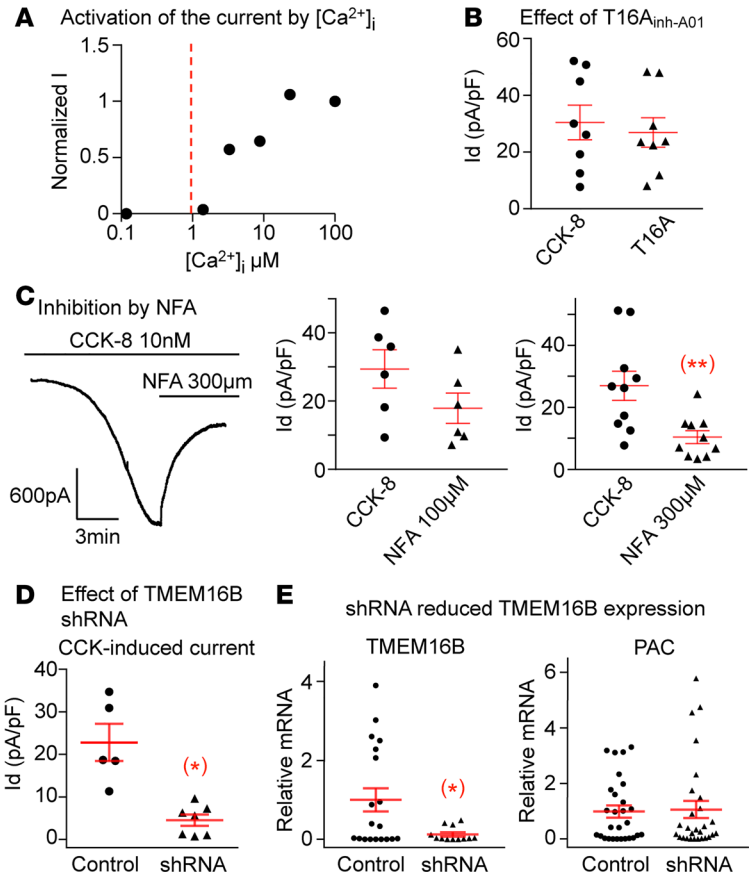

Figure 2. The CCK-8 induced Ca^{2+}-activated Cl^- current is dependent on Ano2/TMEM16B subunit. (**A**) The dose response obtained using 1 excised inside-out patch showed that the Cl^- channel is only activated by Ca^{2+} concentrations higher than 1 μM. (**B**) TMEM16A specific inhibitor $T16A_{inh-A01}$ does not suppress the CCK-8–induced current (n = 8 neurons from 4 ganglia of 2 mice, $P > 0.05$). (**C**) The CCK-8–induced current is reduced from 29.4 ± 5.6 to 17.9 ± 4.4 pA/pF by 100 μM of NFA (n = 6 neurons from 4 ganglia of 2 mice, $P > 0.05$) but is significantly inhibited from 26.9 ± 4.7 to 10.3 ± 2.1 pA/pF (n = 10 neurons from 6 ganglia of 3 mice, $^{**}P < 0.01$) by 300 μM of NFA. (**D**) ShRNA against *Ano2*/TMEM16B greatly reduced the CCK-8–induced current to 4.6 ± 1.3 from 22.8 ± 4.3 pA/pF in control neurons transduced with scrambled sequence (n = 5 and 7 neurons from 4 ganglia of 2 mice, $^{*}P < 0.05$). (**E**) The shRNA reduced the relative mRNA expression of TMEM16B from 1.00 ± 0.30 in control to 0.13 ± 0.01 in shRNA transduced neurons (n = 19 and 12 neurons from 4 ganglia of 2 mice in each group, $^{*}P < 0.05$). The expression of puromycin acetyltransferase (PAC) as an indicator of transduction was similar in both groups (n = 28 neurons from 4 ganglia of 2 mice in each group, $P > 0.05$). Data are presented as means ± SEM, paired (**B** and **C**) or unpaired (**D** and **E**) 2-tailed Student's t test; each data point in the panels represents 1 individual nodose neuron.

channel, the hyposmolarity-induced volume-regulated anion current (SWELL1), which we had identified in nodose neurons (44), is also expressed in labeled intestinal neurons, but its activation is not reduced by HFD (Figure 3G), suggesting that reduction in CCK-induced CaCC current by HFD is selective.

Decreased TMEM16B mRNA expression and CCK-induced CaCC current in nodose neurons of heterozygote mice

To assess the functional contribution of TMEM16B, we reduced its expression by knocking out 1 allele of *Ano2* in NG neurons using a loxP-Cre conditional KO technique. The loxP site flanks either side of exon 12 in *Ano2*. The *Ano2loxP* (*Ano2*$^{fl/fl}$) mice were bred with *Cre* mice expressing Cre-recombinase driven by the $Na_v1.8$ promoter to generate *$Na_v1.8$Cre;Ano2*$^{fl/WT}$ (heterozygote KO) mice with 1 allele of *Ano2* in primary afferent neurons (*Ano2*$^{+/-}$). The littermate *Cre*-negative *Ano2*$^{fl/WT}$ mice were used as WT controls (*Ano2*$^{+/+}$). Both control and *$Na_v1.8$Cre;Ano2*$^{fl/WT}$ mice were born at Mendelian frequency and survived to adulthood.

The decrease of *Ano2* mRNA in nodose neurons of *$Na_v1.8$Cre;Ano2*$^{fl/WT}$ mice was tested using single cell qPCR. The *Ano2* mRNA was 80% lower ($P < 0.05$) in nodose neurons of *$Na_v1.8$Cre;Ano2*$^{fl/WT}$ heterozygote

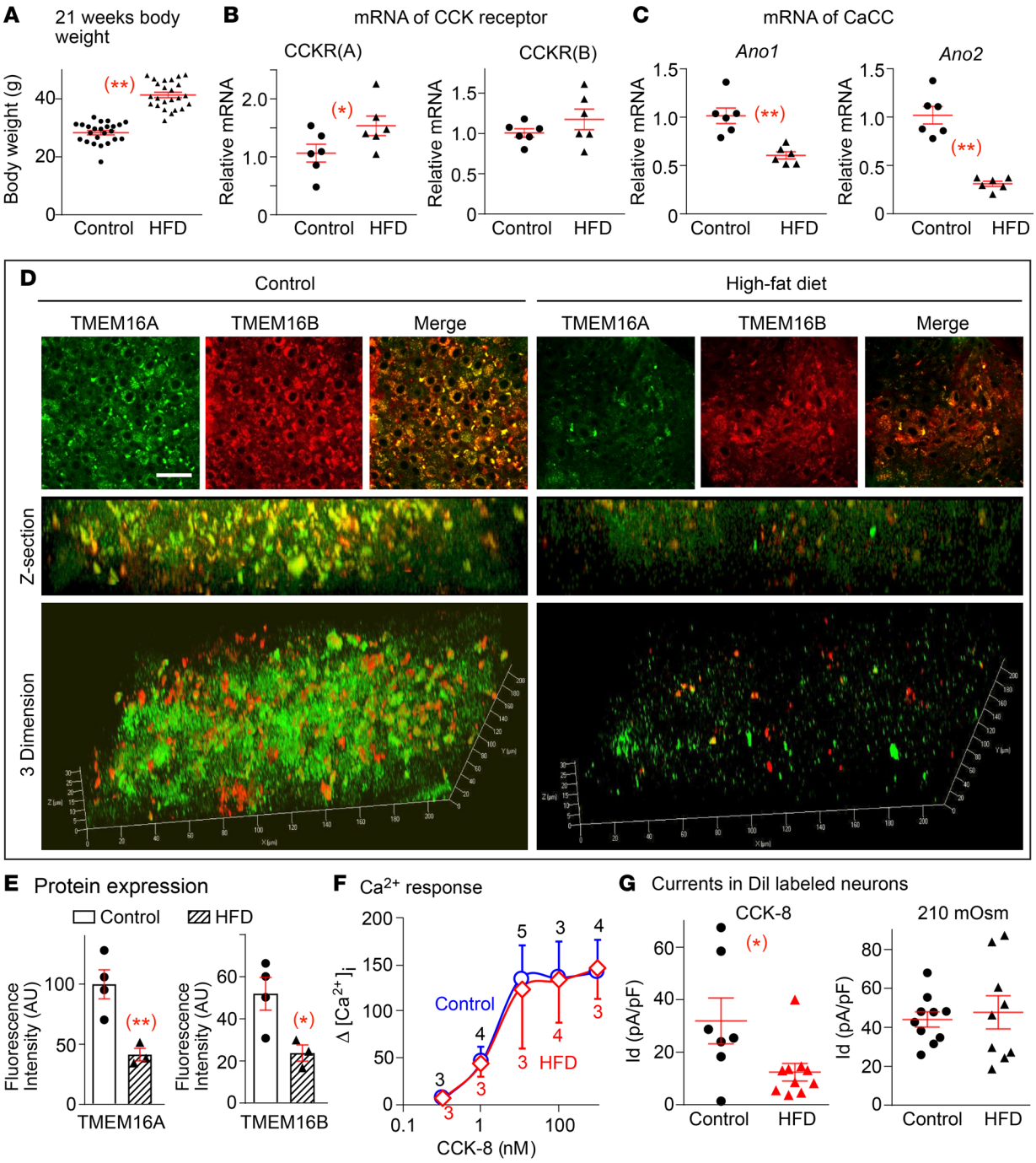

Figure 3. HFD suppresses CCK-8 responses and Ano1 and Ano2 expression in intestinal nodose neurons. (**A**) The body weight of the C57BL/6 mice (n = 24) fed HFD was much greater (41.4 ± 0.9 g, at 20.6 ± 0.4 weeks) than control mice (n = 24) fed regular chow (28.4 ± 0.7 g, at 21.0 ± 0.5weeks, $^{**}P < 0.001$). (**B**) The relative mRNA level of CCK1 receptor (CCKR[A]) in nodose ganglia from mice fed HFD is 1.54 ± 0.41-fold the level from the control group fed regular chow (1.06 ± 0.37, $^{*}P < 0.05$). The level of CCK2 receptor (CCKR[B]) mRNA shows no significant difference between these 2 groups ($P > 0.05$; n = 6 ganglia from 3 mice in each group). (**C**) The mRNA level of *Ano1* is reduced from 1.01 ± 0.20 to 0.61 ± 0.09 fold ($^{**}P < 0.001$), and the *Ano2* level is decreased from 1.02 ± 0.22 (n = 6) to 0.31 ± 0.07-fold ($^{**}P < 0.01$) in ganglia from mice fed regular chow vs. HFD (n = 6 ganglia from 3 mice in each group). (**D**) The protein expression of both TMEM16A (green) and TMEM16B (red) are reduced in nodose ganglia from mice fed HFD compared with regular chow. (**E**) Quantitation showed the fluorescence intensity in mice fed control vs. HFD diet is 99.8 ± 13.8 vs. 41.4 ± 6.4 for TMEM16A and 51.9 ± 9.0 vs. 23.7 ± 4.7 AU for TMEM16B (n = 3–4 slices from 6 ganglia of 3 mice in each group, $^{*}P < 0.05$ and $^{**}P < 0.01$). (**F**) CCK-8–induced increases in $[Ca^{2+}]_i$ are not different in labeled intestinal nodose neurons from mice fed HFD or regular chow (n = 3–5 neurons from 4 ganglia of 2 mice, $P > 0.05$). (**G**) The CCK-8–induced Ca^{2+}-activated Cl^- current (CaCC) in DiI-labeled nodose neurons innervating proximal intestine is attenuated from 32.0 ± 8.7 to 12.4 ± 3.3 pA/pF in mice fed regular chow vs. HFD, respectively (n = 7 and 10 neurons from 4 ganglia of 2 mice, $^{*}P < 0.05$). The osmolarity induced volume-regulated anion channel (VRAC) (SWELL/LRRC8) currents, which are inhibited by DCPIB; however, they show no difference between 2 groups (44.0 ± 3.9 vs. 47.7 ± 8.5 pA/pF in labeled nodose neurons from 8 ganglia of 4 mice fed regular chow vs. 4 ganglia of 2 mice fed HFD, respectively, $P > 0.05$). Each data point represents 1 individual nodose neuron. Data are presented as means ± SEM, unpaired 2-tailed Student's t test.

mice ($Ano2^{+/-}$) compared with their *Cre*-negative $Ano2^{fl/WT}$ littermate controls ($Ano2^{+/+}$). Similarly, the CCK-induced current was reduced by 53.6% ($P < 0.05$ in $Ano2^{+/-}$; Figure 4A).

Increased weight gain in heterozygote mice

Body weight was measured over a 48-week period. Heterozygote $Ano2^{+/-}$ mice gained more weight than littermate controls ($Ano2^{+/+}$). Average maximal body weight of heterozygote ($Ano2^{+/-}$) mice (41.9 ± 1.3 g, $n = 14$) was significantly greater than that of WT littermate control mice (36.0 ± 1.5 g, $n = 14$, $P < 0.0001$; Figure 4B). Increases in body weight of individual mice are reported in Supplemental Figure 1.

CCK-induced Short-term reduction in food intake is reversed in heterozygotes. Since CCK contributes to the satiety signal in vagal afferents, we measured the effect of CCK on food intake in heterozygotes and littermate control mice in metabolic cages after fasting them for 15.5 hours. Immediately at the end of fasting and following i.p. injection of either CCK-8 (3 μg/kg) or saline as control, each mouse was placed back in the cage with free access to food. The amount of food intake was measured every 16 minutes for 4 hours thereafter.

Food intake during the 4 hours after fasting was increased significantly in WT ($Ano2^{+/+}$ mice) given saline but was significantly less after CCK injection compared with saline injection (Figure 4C, left panel). Conversely, during the 4 hours following fasting the heterozygote ($Ano2^{+/-}$) mice receiving saline had a much lower food intake than corresponding control ($Ano2^{+/+}$) mice. Moreover, when injected with CCK-8, the heterozygote mice had a paradoxically greater increase in food intake during the 4 hours after fasting compared with control mice ($Ano2^{+/+}$) injected with saline (Figure 4C).

Metabolic changes in heterozygotes. In addition to the greater increase in weight gain observed over a period of 48 weeks and reversal of the response to CCK-8 with increased short-term food intake, there were other metabolic changes in heterozygote mice compared with control mice ($Ano2^{+/+}$; Figure 5). The fat/lean mass ratio was 0.27 ± 0.07 ($n = 12$) in control mice and 0.31 ± 0.05 ($n = 14$) in heterozygote mice. When the mean value in control $Ano2^{+/+}$ mice was adjusted to exclude 2 outliers of the 12 mice that had fat/lean mass ratios exceeding 3 SDs of the mean of the group, the new ratio of 0.17 ± 0.03 ($n = 10$) in $Ano2^{+/+}$ was significantly reduced compared with that of the heterozygote mice (Figure 5A, $P < 0.05$).

There were significant cumulative decreases ($P < 0.0001$) in energy expenditure (Figure 5C) and in locomotor activity (Figure 5D) in the heterozygote mice ($Ano2^{+/-}$) compared with littermate controls ($Ano2^{+/+}$) that would have contributed to their obesity (Figure 5B). There was also an improvement in glucose tolerance ($P = 0.01$) without a change in insulin tolerance in the heterozygote mice vs. control mice (Figure 5, E and F). Supplemental Table 1 presents detailed analyses of the variance of changes described above.

Neurogenic contribution of CCK-8 to energy expenditure through activation of vagal afferents

The decreased energy expenditure observed in heterozygote mice suggests that the activation of TMEM16B by CCK may also contribute to an increase in thermogenesis. Thus, in addition to CCK-induced satiety, the activation of vagal afferents by CCK may trigger a reflex increase in sympathetic drive to brown adipose tissue (BAT). Such an effect would be abrogated by a HFD and vagotomy. Several studies in rats have identified the role of intestinal vagal afferent neurons in the gut-brain axis regulation of food intake. More specifically, the effect of CCK on these afferents has been described in rats by Raybould and Taché as early as 1988 and by others (45, 46). Since then, studies carried out also in rats have identified the effect of duodenal lipid sensing, as well the effect of glucagon-like peptide-1 released from enteroendocrine cells on nonshivering brown fat thermogenesis (47, 48). Work by our coauthor (CJM) (49, 50) indicates that, in rats, vagal afferent activity can regulate the effect of cooling on BAT sympathetic nerve activity (SNA) and BAT thermogenesis. Given the extensive background information on vagal afferent activation and thermogenesis in BAT that was done in rat models, and our past experience with that model, we used it to determine the effect of CCK-8. It is important that the comparative pharmacology of CCK-induced activation of cultured vagal afferent nodose neurons from rats and mice indicates similar dose dependency, percent responders, and overlap between CCK and capsaicin responsiveness between the 2 species (36). This supports the validity of our interpretation of the metabolic effect of CCK in mice in light of the results obtained in rats.

To determine the role of CCK-induced activation of vagal afferents in the regulation of energy metabolism, we measured SNA to BAT, BAT temperature (T_{BAT}), and expired CO_2 in anesthetized rats while skin temperature (T_{SKIN}) was maintained (35.9°C ± 0.2°C; Figure 6). I.v. injections of CCK-8 (0.5 and 5.0 μg/kg) in rats fed regular chow produced significant increases in BAT SNA, T_{BAT}, and expired CO_2. With the

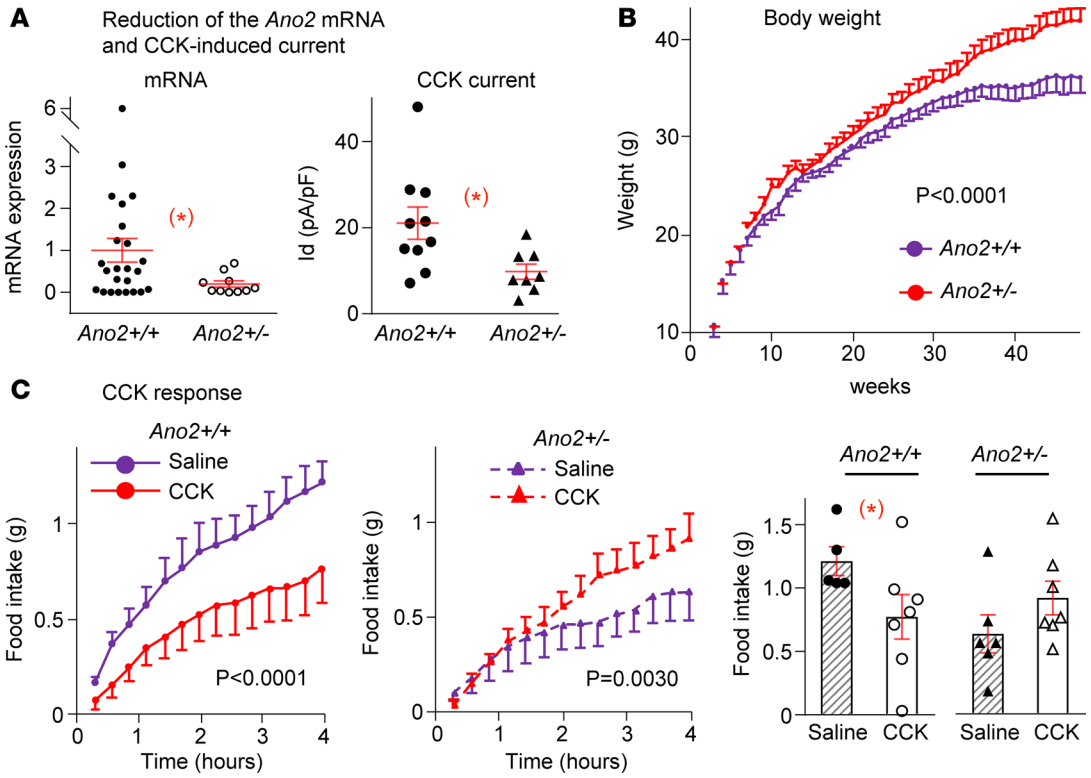

Figure 4. Weight gain and CCK-8 responses of heterozygote TMEM16B-KO mice. (**A**) Conditional KO of *Ano2*/TMEM16B in $Na_v1.8Cre;Ano2^{fl/WT}$ ($Ano2^{+/-}$) mice leads to a significant reduction of mRNA levels in individual nodose neurons compared with littermate controls ($Ano2^{+/+}$), from 1.00 ± 0.28 to 0.20 ± 0.08 (n = 24 and 10 neurons from 8 ganglia of 4 mice for each group, $^*P < 0.05$). The CCK-induced current is significantly reduced from 21.1 ± 3.7 to 9.8 ± 1.8 pA/pF (n = 10 and 8 neurons from 6 ganglia of 3 mice for $Ano2^{+/+}$ and $Ano2^{+/-}$ groups, respectively, $^*P < 0.05$). Unpaired Student's t test. (**B**) The $Ano2^{+/-}$ mice gained more weight, with their maximal body weight averaging 41.9 ± 1.3 g (n = 14) vs. 36.0 ± 1.5 g in control mice (n = 14, $P < 0.0001$, 2-way ANOVA). (**C**) CCK-8 suppresses the cumulative 4-hour food intake following fasting significantly (n = 7) compared with saline (n = 5) in $Ano2^{+/+}$ (left panel, $P < 0.0001$) but increases food intake in $Ano2^{+/-}$ mice (n = 7) compared with saline (n = 6; middle panel, P = 0.0030, 2-way ANOVA). The total 4-hour food intake (bar graph) decreases with CCK from 1.21 ± 0.11 to 0.77 ± 0.18 g ($^*P < 0.05$, unpaired Student's t test) in $Ano2^{+/+}$ and increases from 0.63 ± 0.15 to 0.91 ± 0.13 g ($P > 0.05$, unpaired Student's t test) in $Ano2^{+/-}$ mice. Data are presented as means ± SEM; each symbol represents individual nodose neurons in **A** and represents individual mice in **C**.

high dose of CCK-8 (5 μg/kg), there were transient decreases followed by large and long-lasting (>20 minutes) dose-dependent increases in the 3 responses (Figures 6, A and D).

HFD and bilateral vagotomy each abrogate thermogenic responses to CCK-8. The CCK-induced increases in BAT SNA, T_{BAT}, and expired CO_2 (Figure 6, A and D) were completely abrogated in rats on a HFD (Figure 6, B and D). The responses on normal diet were dependent on vagal afferents, since after bilateral vagotomy, CCK-8 failed to increase BAT SNA and T_{BAT}, while the increase in expired CO_2 was significantly reduced (Figure 6, C and D).

Discussion

The prevalence of obesity and the challenge of effective therapeutic interventions require an understanding of fundamental mechanisms underlying obesity. Vagal intestinal afferents, with cell bodies located in the NG, sense gastrointestinal volume and nutrient content and generate a satiety signal to regulate energy homeostasis. With a paucity of chemical receptors in stomach vagal afferents (51), nutrient contents are primarily detected by the proximal and distal intestines (51). Endocrine I cells located in the mucosa of intestine secrete CCK after intake of protein, fat, and amino acids (52) to activate vagal afferents (15, 16, 45, 53, 54) and regulate short-term food intake (5, 7, 9, 12, 13).

In this study, we report that the activation of intestinal vagal afferents by the satiety signaling peptide CCK requires a potentially novel CaCC subunit, ANO2/TMEM16B. The relevance of this channel to obesity became compelling when we found that obese mice on a HFD have a decreased expression of TMEM16A and TMEM16B, both RNA and protein, in NG — as well as a markedly suppressed CCK-induced CaCC current in DiI-labeled intestinal nodose neurons (Figure 3).

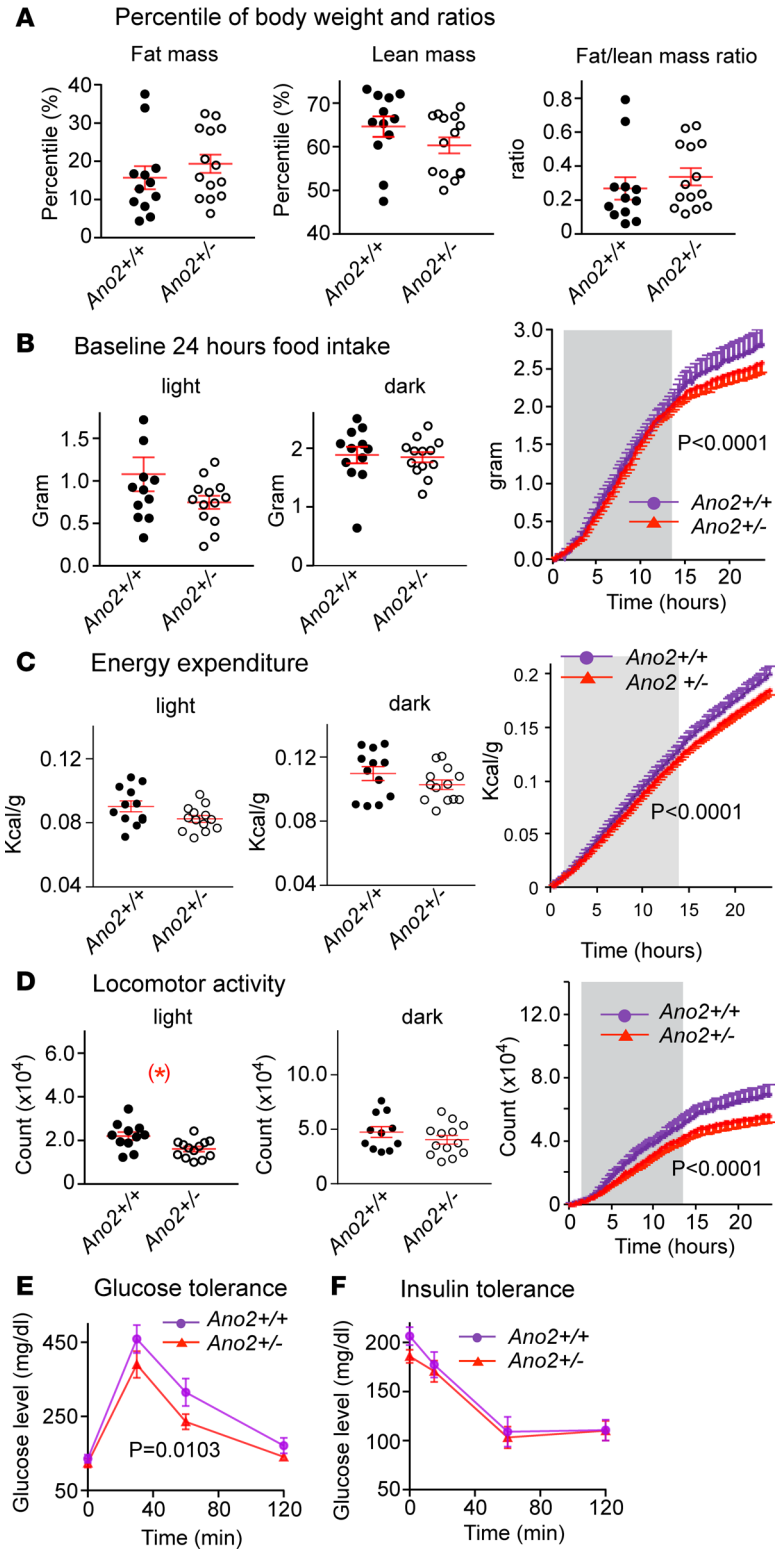

Figure 5. Metabolic changes in *$Na_v1.8$ Cre;Ano2$^{fl/WT}$* (*Ano2$^{+/-}$*) mice. (**A**) The percent body weight in *Ano2$^{+/+}$* vs. *Ano2$^{+/-}$* mice is 15.6% ± 3.3% vs.18.4% ± 2.4% for fat mass, 65.0% ± 2.6% vs.61.1% ± 1.8% for lean mass and 0.267 ± 0.072 vs. 0.314 ± 0.048 for fat/lean mass ratio, respectively (Student's *t* test, $P > 0.05$ for all). By excluding the 2 outliers of the 12 *Ano2$^{+/+}$* mice that had a percent fat mass that exceeded the mean by 3 SD, the calculated fat/lean mass ratio in this control (*Ano2$^{+/+}$*) group decreased to 0.165 ± 0.026, making the increase in fat/lean mass ratio in *Ano2$^{+/-}$* mice significantly greater statistically (Student's *t* test, $P < 0.05$). (**B**) Food intake in control vs. *Ano2$^{+/-}$* mice is 1.08 ± 0.20 vs.0.75 ± 0.08 g ($P > 0.05$) in light phase and 1.88 ± 0.14 g vs.1.84 ± 0.09 g ($P > 0.05$) in dark phase. The 24-hour cumulative food intake shows a significant decrease (right panel, $P < 0.0001$, 2-way ANOVA) mostly during the light phase and is associated with a decrease in locomotor activity. The dark phase (shaded) was between hours 6 p.m. and 6 a.m. (**C**) The energy expenditure of *Ano2$^{+/-}$* mice is reduced in light and dark phases. The cumulative energy expenditure in *Ano2$^{+/-}$* mice is significantly lower as shown during the light phase (unshaded; $P < 0.0001$, 2-way ANOVA). (**D**) The locomotor activity of *Ano2$^{+/-}$* mice is reduced in light and dark phases. The cumulative locomotor activity is decreased in *Ano2$^{+/-}$* mice through the 24-hour period ($P < 0.0001$, 2-way ANOVA). (**E**) The glucose tolerance test shows significantly lower glucose levels in the *Ano2$^{+/-}$* mice at 30, 60, and 120 minutes after glucose injection ($n = 12$ mice in each group, $P = 0.0103$, 2-wayANOVA). (**F**) The insulin tolerance test shows no difference in glucose levels between control and *Ano2$^{+/-}$* mice at 15, 60, and 120 minutes after insulin injection ($n = 12$ for *Ano2$^{+/+}$* and 13 for *Ano2$^{+/-}$* mice, $P > 0.05$, 2-way ANOVA). Data are means ± SEM. Each dot or circle represents 1 mouse. Student's *t* tests are applied in **A** and in the left and middle panels of **B**, **C**, and **D**; 2-way ANOVA are applied to right panels of **B**, **C**, and **D**. More values for locomotor activity, energy expenditure, and glucose and insulin tolerance are presented in Supplemental Table 1.

Obese phenotype of the heterozygotes

To define the function of TMEM16B, 1 allele of the gene was knocked out in sensory neurons using *$Na_v1.8$Cre;Ano2$^{fl/WT}$* mice (*Ano2$^{+/-}$*). Deletion of TMEM16B expression caused a loss of CCK-activated CaCC in nodose neurons and a heterozygote phenotype of increased weight gain and obesity, reversal of the CCK-induced satiety, and significant decreases in energy expenditure and locomotor activity, which likely contributed to weight gain. There was also an increase in fat/lean mass ratio, with some increase in glucose tolerance but without any change in respiratory exchange ratio or sleep time (Supplemental Figure 2).

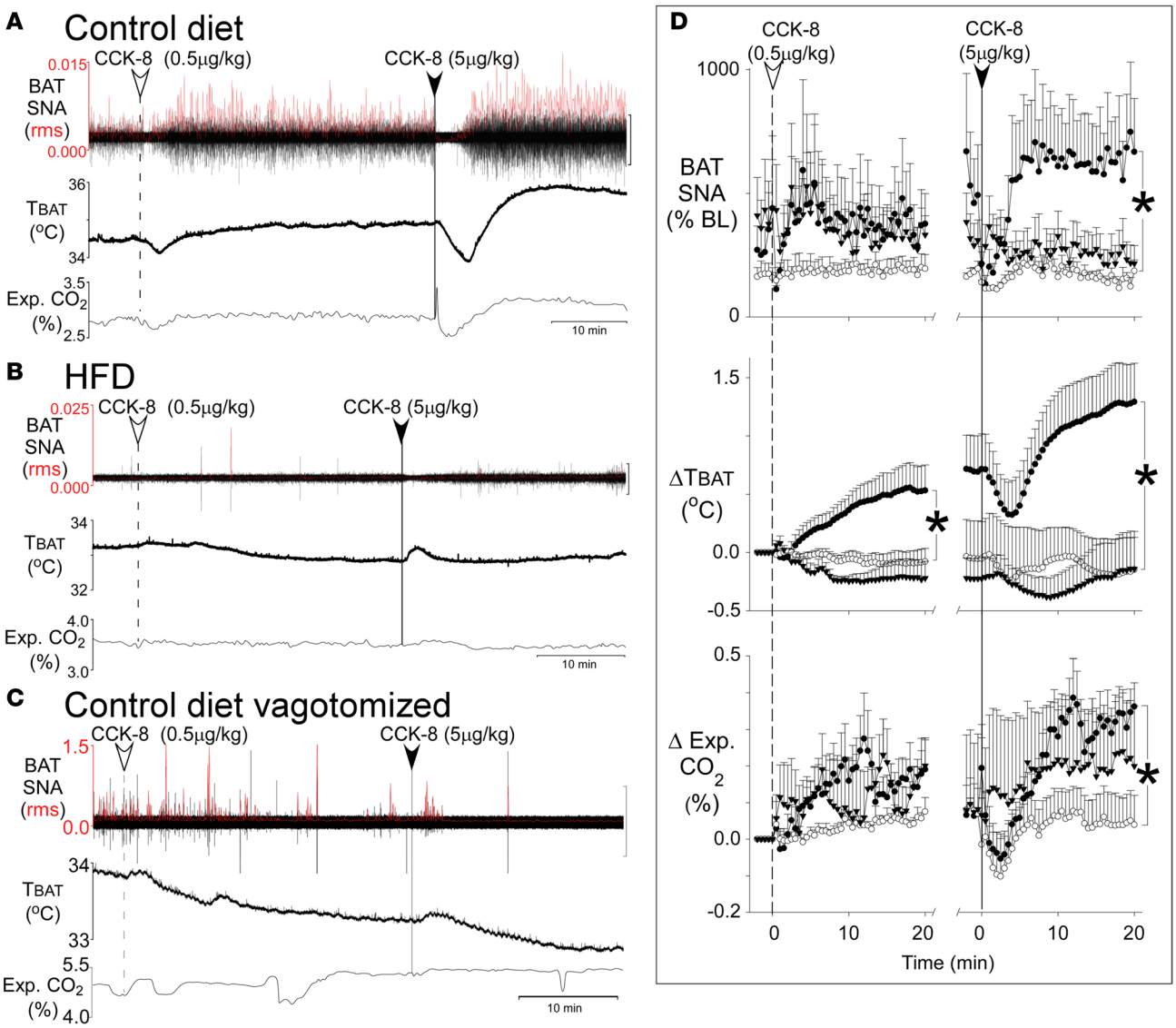

Figure 6. CCK-8 induces thermogenesis in rats fed on control but not in rats fed HFD diet or rats with vagotomy. (**A–C**) The thermogenic responses of individual rats to 2 consecutive i.v. doses of CCK-8 (0.5 μg/kg and 5.0 μg/kg) recorded over a period of 50 minutes. The responses include 3 stimulatory effects of CCK, represented in each panel as increases in brown adipose tissue (BAT) sympathetic nerve activity (SNA root mean square [rms]) in the top tracing, BAT temperature (T_{BAT}) in the middle, and expired carbon dioxide (Exp. CO_2 %) in the lower tracing. (**A**) Pronounced dose-dependent increases in BAT SNA, T_{BAT}, and Exp. CO_2 in a rat on the control diet. (**B**) These responses are eliminated in a rat on the HFD. (**C**) These responses are eliminated in a vagotomized rat on the control diet. SNA amplitude, shown in red, was calculated as the rms value. The black scale bars to the right of the SNA tracings represent 20 μV in **A**, 100 μV in **B**, and 200 μV in **C**. (**D**) The 6 graphs in **D** show group data of the time course of the responses to each of the 2 doses of CCK over a 20-minute period. In each graph, the rats on the control diet (n = 6; filled circles) are compared with rats on the HFD (n = 5; open circles) and to vagotomized rats on the control diet (n = 5; filled triangles). Data are means ± SEM. Each symbol represents the mean value over 30 seconds. Student's t tests were used to compare the 20-minute time point after each CCK injection between rats on the control diet and rats on the HFD. The pronounced increases in BAT SNA, T_{BAT}, and Exp. CO_2 seen with CCK-8 on the control diet were eliminated on the HFD (*P < 0.05). Similarly, vagotomy eliminated SNA and ΔT_{BAT} and suppressed ΔExp. CO_2 responses.

Several aspects of the obese phenotype of heterozygote mice resulting from deletion of *Ano2*/TMEM16B from sensory afferents, and the fact that HFD decreases the expression of that same channel TMEM16B from NG neurons, require further discussion. Our initial impression that a loss of the CCK-mediated activation of intestinal nodose vagal afferents that induce satiety is the cause of obesity in the heterozygotes has limitations.

Contributions of NG vs. DRG neurons. First, deletion of TMEM16B with *Na_v1.8Cre* targets not just NG neurons, but also neurons of dorsal root ganglia (DRG) and trigeminal ganglia. Thus, to the extent that TMEM16B and CCK receptors are expressed in the 3 ganglia, the CCK-mediated response may not be

solely ascribed to nodose vagal afferents. To address that issue at least in part, we contrasted the mRNA expression of CCK receptors and Ano1 and -2 subunits in DRG vs. NG. As demonstrated in Supplemental Figure 3, A and B, the expression of *Ano2*, CCK1, and CCK2 receptors are significantly lower in DRG than in NG. Moreover, the magnitude of the CCK-induced CaCC currents (*Ano*2/TMEM16B) is significantly less in DRG than NG. One might therefore attribute a greater extent of the CCK-induced sensory activation to intestinal vagal afferents of nodose neurons than DRG neurons.

Reversal of satiety response. An unexpected finding is the reversal of the CCK-8 satiety response in the heterozygote mice. To our surprise, CCK-8 receptor activation in the heterozygote mice not only failed to suppress food intake, as seen in littermate control mice, but caused a paradoxical increase in food intake and seemed to switch the long-term effects of CCK from anorexigenic to orexigenic. The possibility of a central action of CCK-8 was considered, since CCK-8 has been reported to activate orexin/hypocretin neurons through CCK1 (CCKA) receptors (55). Orexins have been implicated in regulating sleep/wakefulness and increases in food intake and locomotor activity when administered centrally to animals (56–58). Conflicting studies have reported that CCK suppressed food intake (59–61) as well as locomotor activity (62) when administered i.p. or intracerebroventricularly, making it difficult to define the central contribution.

An alternative to the central effect is the CCK-induced increase in $[Ca^{2+}]_i$ in nodose neurons, which — in the absence of TMEM16B— may open the Ca^{2+}-activated potassium channel (I_{KCa2+}). This activation causes hyperpolarization and suppression of any tonic vagal afferent activity and, thus, would favor increased food intake. Such coactivation of CaCC and I_{KCa2+} by carbamylcholine has been reported in isolated lacrimal gland cells (63). Thus, the enhanced food intake noted in the heterozygote mice might reflect sequential activation of CCK1 (CCKA) receptors, an increase in $[Ca^{2+}]_i$, activation of I_{KCa2+}, and hyperpolarization of satiety-inducing vagal afferents. Supporting this theory is the finding that reversal of the CCK satiety effect depends on activation of the CCK receptor and is not seen in CCK1 (CCKA) receptor–KO male mice (60).

Vagal afferents, thermogenesis and energy expenditure

The metabolic response with decreased energy expenditure in heterozygote mice (*Ano2*$^{+/-}$) raised the possibility that CCK-induced vagal afferent activation of TMEM16B may induce thermogenesis, which heretofore has not been reported, to our knowledge. Several reports have indicated that CCK and vagal afferent activity can modulate thermogenesis in addition to food intake and satiety and, thus, define the magnitude of energy expenditure and weight gain (48, 50, 64–67). Figure 6 demonstrates that i.v. CCK-8 (0.5 μg/Kg and 5.0 μg/Kg) infused over a period of 50 minutes significantly increases SNA in BAT in rats. This effect would complement the effect of CCK on satiety with an increase in energy metabolism and thermogenesis in BAT (50). Since these responses were abrogated by vagotomy, we conclude that they were mediated by CCK-sensitive vagal afferents. Of interest, CCK-sensitive vagal afferents are also activated by duodenal lipids that enhance BAT thermogenesis through activation of CCK1 (CCKA) receptors (48).

The significant decrease in expression of TMEM16B in NG and the loss of CCK sensitivity of mice fed a HFD highlights 2 effects that favor increased body weight. One is the decreased satiety response and unmasking of an orexigenic effect of CCK, as mentioned above. The second effect is the loss of CCK-mediated activation of vagal afferents, which abrogated increases in SNA and thermogenesis in BAT and decreased energy metabolism (Figure 6B) (50, 64). Taken together with our finding that heterozygote mice exhibit CCK insensitivity and decreased energy expenditure, our results suggest that activation of TMEM16B by CCK in vagal afferents may evoke the reflex increases in BAT SNA and thermogenesis. Impaired sympathetic activation during HFD intake and impaired thermogenesis in BAT are likely important contributors to weight gain in obese adult humans (65, 66). Even the decreased locomotor activity in heterozygote mice may be a consequence of CCK insensitivity, as reported by Hirosue et al. (62), who show that CCK antagonists induced suppression of locomotor activity in mice.

Decreased expression of TMEM16 on HFD. In obese mice on a HFD, we found a significant decrease in expression of TMEM16 in NG, which reduced CCK-induced firing of intestinal afferents and satiety (17) despite significant increases in CCK levels and CCK1 (CCKA) receptors (23, 24, 68). The reason for the decreased expression of TMEM16 on HFD is unclear. A consideration is that long- and short-chain fatty acids regulate gene expression in many mammalian cells and tissues (69). Long-term consumption of a HFD in mice decreases expression of peroxisome proliferator-activated receptors (PPARγ) in NG, and conditional KO of PPARγ in NG neurons induces weight gain (67). Consequently, if TMEM16 is regulated by PPARγ in nodose neurons, its suppression by a HFD would be expected as a result of the decrease in PPARγ.

We observed changes in baseline 24-hour cumulative food intake that appear to conflict with the CCK-induced food intake and pattern of weight gain (Figure 5B). In the heterozygote mice that became obese, 24-hour food intake was reduced, whereas CCK administration enhanced food intake during the period of 4 hours following 15.5 hours of food deprivation. CCK is a regulator of short-term food intake, whereas the baseline 24-hour cumulative food intake obtained at the end of the 48-week study reflects both short- and long-term control of intake, as well as the effects of changes in energy metabolism and locomotor activity. Moreover, the relative decline in 24-hour intake was evident during the light phase in heterozygote mice when their locomotor activity was markedly reduced.

Although we ascribe the weight gain phenotype to the decrease of *Ano2* expression in intestinal vagal afferents to nodose neurons specifically in response to CCK, we cannot exclude the effects of CCK on central orexigenic or anorexigenic central neurons. We also cannot exclude the potential effect of *Ano2* deletion in peripheral sensory neurons on response of vagal afferents to other ligands, which regulate metabolism, heat generation, locomotor activity, and long-term 24-hour food intake.

Perspective

We have identified TMEM16B the anoctamin CaCC in intestinal vagal afferent neurons as the neuronal sensor of CCK-induced satiety. We suggest that it is a potentially novel regulator of weight gain and its suppression by HFD contributes to obesity. Based on our findings, the *Ano2*/TMEM16B may serve as a new therapeutic target for obesity in the future. Therapeutic strategies targeting type 1 CCK receptors (CCKR[A]) or enhancing CCK receptor sensitivity have not been successful (5). The doses of such drugs used to cause weight loss are high and cause significant side effects. Our studies suggest that decreased expression of CaCC channels downstream of CCK receptors may serve as a rate-determining step to limit the response of vagal afferents to those drugs. Future strategies should preferentially target CaCC channel expression to restore and enhance the impaired vagal afferent sensing mechanism.

Methods

Animals, diet, body weight, and metabolic studies

C57BL/6 male mice (The Jackson Laboratory) were used unless otherwise indicated. All animals were euthanized according to NIH/American Physiological Society (APS) guidelines under anesthesia followed by cervical dislocation after completion of each protocol. Animals were housed in a 12:12-hour light-dark cycle with free access to food (regular chow, EVIGO 7913) consisting 18% calories from fat and 23% from protein (3.1 kcal/g) and water ad libitum. Key resources that were used for all materials and animals are listed in the Supplemental Table 2.

Studies of the effect of HFD were done in male C57BL/6 mice (starting at 6–8 weeks of age) fed a diet (D12492, Research Diets Inc.) consisting of 60% calories from fat and 20% from protein (5.24 kcal/g) for a total of 12–14 weeks. Control littermates were fed regular chow.

Studies on heterozygote TMEM16B $Na_v1.8Cre;Ano2^{fl/WT}$ male mice (C57BL/6-129/Svj background) ($Ano2^{+/-}$) and their littermate controls ($Ano2^{+/+}$) were carried out over a period of 1 year. Body weight was recorded weekly. Animal care was supervised by veterinarians in our animal care facilities. Metabolic studies and monitoring of food intake and activities with CCK-8 injection were done in facilities that included a Comprehensive Lab Animal Monitoring System (CLAMS).

The sample size for our animal experiments was estimated based on the variability of the responses in our pilot experiments. We have used all living heterozygote mice and their littermate controls and did not exclude any mice to avoid bias.

Dissociation and culture of neurons

Thoracic DRG (thoracic vertebrae levels 10–13; T10-13) and NG neurons were cultured as described previously (44). Mice were anesthetized with 3%–5% isoflurane. NG and DRG were removed and digested with DMEM/F12 media containing 1% penicillin/streptomycin, 10 mM HEPES (all from Thermo Fisher Scientific), supplemented with DNAse (0.1 mg/ml), trypsin (1 mg/ml), and collagenase (1 mg/ml) (all from Worthington). DMEM media (Thermo Fisher Scientific) containing BSA (1 mg/ml, RPI) was added after digestion. Cells were centrifuged and resuspended in culture medium

containing DMEM/F12, 10 mM HEPES, penicillin/streptomycin, and 10% fetal bovine serum (FBS, Thermo Fisher Scientific), and transferred to glass coverslips coated with poly-L-lysine (Thermo Fisher Scientific) and incubated at 37°C overnight.

DiI labeling of intestinal neurons. Mice were anesthetized, and DiI (50 mg/ml; Molecular Probes) was injected into the submucosa of the duodenal and jejunal intestine. Animals were euthanized 2–4 weeks after DiI labeling. DiI-labeled nodose neurons were cultured and identified using FITC filter set (excitation and emission wavelength [Ex/Em] 490/525 nm) on the microscope stage (Nikon).

Measurement of ionic currents in nodose neurons. Currents of cultured nodose neurons were recorded using the whole-cell voltage-clamp technique, as described previously (44), using Axopatch 200B amplifier and pCLAMP 8 software (Axon Instruments). Pipette solution contained (mM): 121 KCl, 10 NaCl, 2 $MgCl_2$, 10 HEPES (all from RPI), 5 EGTA, 2 K_2-ATP (Both from MilliporeSigma) (pH 7.2) adjusted with 1 M tetramethylphenyl-ammonium hydroxide (TMAOH, MilliporeSigma). Perfusion solution contained (mM):124 NaCl, 5.4 KCl, 2 $CaCl_2$, 1 $MgCl_2$, 10 HEPES, 10 MES (MilliporeSigma), 5.5 glucose (RPI) (pH 7.4 and 7.0, 6.5, and 6.0) adjusted with TMAOH. Current was measured with Clamfit 9.2 (Axon Instruments).

Calcium imaging. As described previously (70), neurons were loaded with 5 μM Fluo-4/AM (Invitrogen, Molecular Probes) for 30 minutes. Fluorescence images were obtained using a filter cube (c-FL HYQ FITC) with Ex/Em of 535 ± 50 nm and 480 ± 40 nm on an inverted fluorescence microscope (Nikon TE2000-U) with 10-ms exposure time and a 1- to 5-second sampling interval. The 12-bit digital cooled charge-coupled device (CCD) camera (Cool SNAP-cf, Photometrics) was used with the graphics control software package MetaMorph 6.1.3. Fluorescence intensity (F) was converted to $[Ca^{2+}]_i$ in individual neurons using the equation: $[Ca^{2+}]_i = K_d (F - F_{min})/(F_{max} - F)$, where K_d = 345 is the dissociation constant (71).

Bath solution (pH 7.4) contained the following in mM: 136.9 NaCl, 5.4 KCl, 4.2 $NaHCO_3$, 1.3 $CaCl_2$, 0.8 $MgSO_4$, 0.4 NaH_2PO_4, 5.6 D-glucose, and 10 HEPES. CCK-8 (MilliporeSigma) 0.1 to 1000 nM was diluted in bath solution. Calcium ionophore, 20 μM ionomycin, and 2 mM EGTA (MilliporeSigma) were used to determine maximum and minimum fluorescent intensity (F_{max} and F_{min}).

Real-time PCR

Total RNA was extracted from mouse tissues using Trizol reagent (Invitrogen) and chloroform and treated with Ambion's DNase Treatment Kit (Thermo Fisher Scientific) to remove possible DNA contamination. Total RNA was further purified by Rneasy Column Purification kit (Qiagen's Rneasy Protocol). RNAs were reverse transcribed into cDNA using AffinityScript QPCR cDNA Synthesis Kit (Agilent Technologies). qPCR was performed using Brilliant SYBR Green QPCR Master Mix (Agilent Technologies) with ABI 7000 real-time PCR system (Conquer Scientific). Specific primers were purchased from Integrated DNA Technologies (IDT). Expression of GAPDH was used to normalize measurements. Data were analyzed using the $\Delta\Delta C_T$ method. Primer sequences used for real-time PCR are listed in Supplemental Table 3.

Single cell RT-PCR. Single cell reverse transcription PCR (RT-PCR) was performed as previously described (72). Individual cultured nodose neurons were aspirated into a glass microcapillary tube (~25 μm) and lysed with 4.5 μl lysis buffer containing 0.3% IGEPAL CA-630 (I8896, MilliporeSigma), 150 mM NaCl (Invitrogen), 10 mM Tris-HCl (Invitrogen), and 0.1% BSA (A8412, MilliporeSigma). RT-PCR was done as noted above, except that the threshold for positive mRNA expression was 50 instead of 40 cycles. The RT-PCR product was validated by a single band on the gel and DNA sequencing analysis (Iowa Institute of Human Genetics, Genomics Division, University of Iowa). Primers used are: *Ano2* forward, 5′-CCA GAA TGC CTT CAC CAT GT-3′; *Ano2* reverse, 5′-AAC CGC ATC TGG AGT CTC TT-3′; PAC forward, 5′-CTCGACATCGGCAAGGTGTG-3′; PAC reverse, 5′-GAACCGCTCAACTCGGCCAT-3′.

Immunohistochemistry

Anesthetized mice were perfused with ice-cold fixative (4% paraformaldehyde in phosphate buffered saline, PBS; Thermo Fisher Scientific). NG in OCT was rapidly frozen using liquid nitrogen and sliced into 10-μm sections. After treatment with primary antibodies (1:50) and secondary antibodies (1:200), slides were mounted and images were taken with an inverted Bio-Rad 1024 laser scanning confocal microscope equipped with Argon lasers (488 and 514 nm) and helium-neon (543 nm) and analyzed using ImageJ (NIH)software.

Primary antibodies. Goat polyclonal anti-*Ano1* (catalog sc-69343, lot E2714), which recognizes epitope amino acids 825–875 of human *Ano1*, is validated by Sun et al. (73) in pulmonary artery protein lysates and several labs in other tissues (74–79). It shows a band of approximately 114 kDa in Western blot.

Rabbit polyclonal anti-*Ano2* (catalog sc-292004, lot E2813), which recognizes amino acids 931–1003 of human *Ano2*, has been validated by Dibattista et al. (80) on HEK 293T cells transiently transfected with plasmids containing *Ano2* cDNA. This antibody recognized *Ano2* and showed no cross-reaction to *Ano1*.

Fluorescence conjugated secondary antibodies were donkey anti-goat (sc-2024) and mouse anti-rabbit (sc-3917) (both from Santa Cruz Biotechnology Inc.).

Na_v1.8Cre;Ano2$^{fl/WT}$ Mice. *Ano2$^{fl/fl}$* mice (*Ano2* , GenBank AC122284.5) with C57BL/6-129/Svj background were provided by Thomas J. Jentsch's lab (Leibniz-Institut für Molekulare Pharmakologie [FMP]/Max-Delbrück-Centrum für Molekulare Medizin [MDC], Berlin, Germany) (81). The *Na_v1.8Cre* mice (Cre, EMBL X03453.1) were provided by John N. Wood's lab (Wolfson Institute for Biomedical Research, University College London, United Kingdom) (82). These mice express Cre-recombinase in Na_v1.8-positive sensory neurons such as NG, dorsal root ganglia, and trigeminal ganglia (83). The *Ano2$^{fl/fl}$* mice were crossed with *Na_v1.8Cre* mice to generate *Na_v1.8Cre;Ano2$^{flox/WT}$* mice. The genotype of these mice was tested using PCR with primers: Cre forward, 5′-TGC CTG CAT TAC CGG TCG AT-3′; Cre reverse, 5′-ATC CGC CGC ATA ACC AGT GA-3′. The *Ano2* was tested by primers: forward, 5′-GGA CAC CCC GTA CTT GAA GA-3′; reverse, 5′-AGC ACA ATG CAG ACC AAG TT-3′.

ShRNA transduction. The lentivirus carrying shRNA against TMEM16B (sc-154400-V, Santa Cruz Biotechnology Inc/) contained a mixture of 3 different shRNA plasmids. Hairpin sequence of plasmid A is: 5′-GATCCGCATTGTACACGAGATTCTTTCAAGAGAAGAATCTCGTGTACAATGCTTTTT-3′; plasmid B is: 5′-GATCCCAAGTTCTCCGTCATCATTTTCAAGAGAAATGATGACGGAGAACTTGTTTTT-3′; plasmid C is: 5′-GATCCCATCCTAGCACCCATCTAATTCAAGAGATTAGATGGGTGCTAGGATGTTTTT-3′.

shRNA was transduced according to the protocol by Santa Cruz Biotechnology Inc. Cultured nodose neurons was treated with lentivirus containing shRNA or empty vector (~1000 MOI) for 6–7 hours. Transduced neurons were selected with puromycin (3 μg/ml) 2 days after transduction. Reduction of mRNA was tested with qPCR 2 days after application of puromycin, and currents were recorded after 4–5 days. The concentration of puromycin was determined by adding 0.5–10 μg/ml of puromycin (44).

Comprehensive monitoring system

The *Na_v1.8Cre;Ano$^{fl/WT}$* mice and their control littermates without Cre at 1 year of age were housed in individual chambers of the CLAMS (Columbus Instruments) for measurements of energy expenditure, locomotor activity, indirect calorimetry, and 24-hour food intake (84). Mice were monitored continuously for 5 days. Data obtained at days 3–5 were used. Mice were fasted for 15.5 hours with free access to water between 4:30 p.m. and 8:00 a.m. They were then injected i.p. with either CCK (3 μg/kg body weight) or saline at 8:00 a.m. on day 5 and rehoused in CLAMS chambers with free access to food and water. Food intake was measured over the subsequent 4 hours.

Nuclear magnetic resonance (NMR). The body fat mass and lean mass ratios were assessed using NMR (Minispec LF50, Bruker) 1 week after the CLAMS study. Mice were placed in a polycarbonate restraint tube and scanned for a rapid analysis (approximately 1 minute).

Glucose and insulin tolerance tests. Glucose and insulin tolerance were tested 1 week after NMR study. Mice were fasted for 16 hours and then weighed and slightly sedated using 3% isoflurane. Tail blood was dropped on the test strip (catalog 1620911, Abbott Laboratories) of the glucose meter (catalog CFGS293-M1652, Abbott Laboratories) to test the baseline glucose level (time 0). Mice were then injected i.p. with glucose (2 g/kg body mass, 20% glucose, MilliporeSigma) (85). Glucose levels were measured 30, 60, and 120 minutes after injection.

One week after the glucose tolerance test, mice were fasted for 6 hours in the morning and then weighed, and baseline blood glucose level was measured. Mice were injected i.p. with insulin (0.75×10^{-3} U/g body mass). Glucose levels were measured 15, 60, and 120 minutes after injection.

SNA and thermogenesis in BAT

Male Wistar rats (Charles River Laboratories) were housed at 22°C–23°C in a 12:12-hour light-dark cycle with free access to water and control diet (n = 11, 13% kcal from fat; Laboratory Rodent Diet 5001, LabDiet.com) or HFD (n = 5, 45% kcal from fat; Research Diets, D1245) and were maintained for 53 ± 13 days after their body weight reached 300 g. Rats were anesthetized with isoflurane (Phoenix) (2%–3% in 100% O_2) and the femoral artery, and vein and trachea were cannulated (60). Rats were then kept

anesthetized with urethane (750 mg/kg i.v.) and α-chloralose (60 mg/kg i.v.), artificially ventilated with oxygen, and paralyzed with d-tubocurarine. Expired CO_2 was measured using a capnometer (CapStar 100, CWE Inc.). T_{BAT}, T_{SKIN}, and core body temperature (T_{CORE}) were measured via thermocouples in the interscapular BAT pad, on the hindquarter skin, and in the rectum, respectively. BAT SNA was recorded with bipolar hook electrodes, amplified (×10,000), filtered (1–300 Hz), and digitized to a hard drive (Spike 2; Cambridge Electronic Design).

BAT SNA was quantified using Spike2 software. SNA amplitude was calculated as the square root of the total power in the 0.1–20 Hz frequency band (root mean square value) from the autospectra of sequential 4-second segments of BAT SNA. Values of BAT SNA were normalized to a baseline level taken as the mean BAT SNA amplitude during a 2-minute period of minimum BAT SNA recorded (T_{CORE} and T_{SKIN} > 36.5˚C). Rats on the control diet were i.v. injected with CCK 0.5 μg/kg, and a second dose of 5 μg/kg was injected 20–30 minutes later (n = 6). A separate group of rats (n = 5) with the same injection was vagotomized bilaterally at the cervical level after tracheal cannulation.

Chemicals/solutions/drugs. NFA (MilliporeSigma, N0630) and $T16A_{inh\text{-}A01}$ (MilliporeSigma, 613551) were dissolved in DMSO. CCK-8 (MilliporeSigma, C2175, or Tocris Bioscience, 1166) was dissolved in water. BAPTA with 1 M concentration was dissolved in a pipette solution to 10 mM, and the pH was adjusted to 7.25 using HCl. The osmolarity was measured after pH adjustment with a vapor pressure osmometer (Wescor). The extracellular free Ca^{2+} concentration was calculated according to the program MaxChelator (Stanford University, Stanford, California, USA).

Statistics. Data were presented as means ± SEM. Significance of responses was analyzed with 2-tailed Student's t tests or 2-way ANOVA using Excel, GraphPad Prism6, and SYSTAT software. Values of $P < 0.05$ were considered significant. In testing the effects of various pharmacological blockers, the CCK-8 responses with and without the blocker were obtained from the same nodose neurons and the differences were tested using paired Student's t test.

Study approval. All animal maintenance and handling and experimental protocols were approved by the University of Iowa IACUC or by the Oregon Health & Science University IACUC, as required. The ethical conduct in the care and use of animals followed NIH/APS guidelines.

Author contributions

RW contributed to all experiment design and conducted the patch-clamp and behavior experiments, analyzed and interpreted data, and wrote the manuscript. YL also contributed substantially to the design, generating and confirming the conditional KO mice of *Ano2* in nodose neurons on loxP-Cre system, including genotyping and sequencing; to the design and conduct of experiments to detect the mRNA and protein levels of *Ano1* and *Ano2* using qPCR, single cell PCR, and IHC; and to the detection of the dose dependence of CCK response by using intracellular calcium imaging. MZC dissected all neurons, generated and maintained the *Na_v1.8Cre;Ano2$^{fl/WT}$* mouse line, and designed and conducted the glucose and insulin tolerance tests. MVS designed and conducted the glucose and insulin tolerance experiments. CJB contributed to the original design and edited the manuscript. CJM designed and conducted the experiments on sympathetic nerve activity in rat BAT, BAT thermogenesis, and expired CO_2. MWC contributed to the experimental design, result interpretation, and manuscript editing. FMA developed the hypotheses and contributed to the experimental design, reviewed and interpreted the results, and wrote the manuscript.

Acknowledgments

We thank Thomas J. Jentsch and Gwendolyn M. Billig from Leibniz-Institut für Molekulare Pharmakologie (FMP; Berlin, Germany) for the *Ano2$^{fl/fl}$* mice, John N. Wood from University College (London, United Kingdom) for the *Na_v1.8Cre* mice; Kristina K. Greiner for editing for clarity and consistency; Angela M. Hester and Monica H. Kopet for assistance with word processing and manuscript preparation; Shawn Roach for assistance with editing the figures; Michael J. Welsh for the use of laboratory facilities and consultation; and Jamie E. Soto in the Metabolic Phenotyping Core Facility for conducting the metabolic cage experiments. We also thank the University of Iowa DNA Facility, Central Microscopy Research Facility, and Office of Animal Resources for support.

The work was supported by Program Project grant HL014388-42 from the NIH (FMA, MWC, and CJB), Department of Veterans Affairs VA Merit Review Award 1 BX001414 (MWC), American

Diabetes Association Basic Science Grant 1-13-BS-120 (CJM), NIH R01-DK112198 (CJM), and the NHLBI T32 Iowa Cardiovascular Interdisciplinary Research Fellowship HL007121 (RW).

Address correspondence to: François M. Abboud or Runping Wang, Abboud Cardiovascular Research Center, 501 Newton Road, University of Iowa, Iowa City, Iowa, USA. Phone: 319.335.7708; Email: francois-abboud@uiowa.edu (FA). Phone: 319.335.7684; E-mail: runping-wang@uiowa.edu (RW).

1. Pi-Sunyer X. The medical risks of obesity. *Postgrad Med*. 2009;121(6):21–33.
2. Must A, Spadano J, Coakley EH, Field AE, Colditz G, Dietz WH. The disease burden associated with overweight and obesity. *JAMA*. 1999;282(16):1523–1529.
3. Kim S. Drugs to treat obesity: do they work? *Postgrad Med J*. 2016;92(1089):401–406.
4. Hellström PM. Satiety signals and obesity. *Curr Opin Gastroenterol*. 2013;29(2):222–227.
5. Miller LJ, Desai AJ. Metabolic Actions of the Type 1 Cholecystokinin Receptor: Its Potential as a Therapeutic Target. *Trends Endocrinol Metab*. 2016;27(9):609–619.
6. Davenport RJ, Wright S. Treating obesity: is it all in the gut? *Drug Discov Today*. 2014;19(7):845–858.
7. Strader AD, Woods SC. Gastrointestinal hormones and food intake. *Gastroenterology*. 2005;128(1):175–191.
8. Kentish SJ, Page AJ. The role of gastrointestinal vagal afferent fibres in obesity. *J Physiol (Lond)*. 2015;593(4):775–786.
9. Geary N. A physiological perspective on the neuroscience of eating. *Physiol Behav*. 2014;136:3–14.
10. Covasa M, Ritter RC. Rats maintained on high-fat diets exhibit reduced satiety in response to CCK and bombesin. *Peptides*. 1998;19(8):1407–1415.
11. Maggio CA, Haraczkiewicz E, Vasselli JR. Diet composition alters the satiety effect of cholecystokinin in lean and obese Zucker rats. *Physiol Behav*. 1988;43(4):485–491.
12. Overduin J, Gibbs J, Cummings DE, Reeve JR. CCK-58 elicits both satiety and satiation in rats while CCK-8 elicits only satiation. *Peptides*. 2014;54:71–80.
13. Sayegh AI, Washington MC, Raboin SJ, Aglan AH, Reeve JR. CCK-58 prolongs the intermeal interval, whereas CCK-8 reduces this interval: not all forms of cholecystokinin have equal bioactivity. *Peptides*. 2014;55:120–125.
14. Beglinger C, Degen L, Matzinger D, D'Amato M, Drewe J. Loxiglumide, a CCK-A receptor antagonist, stimulates calorie intake and hunger feelings in humans. *Am J Physiol Regul Integr Comp Physiol*. 2001;280(4):R1149–R1154.
15. Székely M. The vagus nerve in thermoregulation and energy metabolism. *Auton Neurosci*. 2000;85(1-3):26–38.
16. Ueno H, Nakazato M. Mechanistic relationship between the vagal afferent pathway, central nervous system and peripheral organs in appetite regulation. *J Diabetes Investig*. 2016;7(6):812–818.
17. Daly DM, Park SJ, Valinsky WC, Beyak MJ. Impaired intestinal afferent nerve satiety signalling and vagal afferent excitability in diet induced obesity in the mouse. *J Physiol (Lond)*. 2011;589(Pt 11):2857–2870.
18. Sarri E, Ramos B, Salido GM, Claro E. The cholecystokinin analogues JMV-180 and CCK-8 stimulate phospholipase C through the same binding site of CCK(A) receptor in rat pancreatic acini. *Br J Pharmacol*. 2001;133(8):1227–1234.
19. Yule DI, Tseng MJ, Williams JA, Logdson CD. A cloned CCK-A receptor transduces multiple signals in response to full and partial agonists. *Am J Physiol*. 1993;265(5 Pt 1):G999–1004.
20. Matozaki T, Williams JA. Multiple sources of 1,2-diacylglycerol in isolated rat pancreatic acini stimulated by cholecystokinin. Involvement of phosphatidylinositol bisphosphate and phosphatidylcholine hydrolysis. *J Biol Chem*. 1989;264(25):14729–14734.
21. Lankisch TO, Tsunoda Y, Lu Y, Owyang C. Characterization of CCK(A) receptor affinity states and Ca(2+) signal transduction in vagal nodose ganglia. *Am J Physiol Gastrointest Liver Physiol*. 2002;282(6):G1002–G1008.
22. Wu SV, Harikumar KG, Burgess RJ, Reeve JR, Miller LJ. Effects of cholecystokinin-58 on type 1 cholecystokinin receptor function and regulation. *Am J Physiol Gastrointest Liver Physiol*. 2008;295(3):G641–G647.
23. Paulino G, et al. Increased expression of receptors for orexigenic factors in nodose ganglion of diet-induced obese rats. *Am J Physiol Endocrinol Metab*. 2009;296(4):E898–E903.
24. Spannagel AW, Nakano I, Tawil T, Chey WY, Liddle RA, Green GM. Adaptation to fat markedly increases pancreatic secretory response to intraduodenal fat in rats. *Am J Physiol*. 1996;270(1 Pt 1):G128–G135.
25. Little TJ, et al. A high-fat diet raises fasting plasma CCK but does not affect upper gut motility, PYY, and ghrelin, or energy intake during CCK-8 infusion in lean men. *Am J Physiol Regul Integr Comp Physiol*. 2008;294(1):R45–R51.
26. Vasconcelos LH, Souza IL, Pinheiro LS, Silva BA. Ion Channels in Obesity: Pathophysiology and Potential Therapeutic Targets. *Front Pharmacol*. 2016;7:58.
27. Park SJ, Yu Y, Wagner B, Valinsky WC, Lomax AE, Beyak MJ. Increased TASK channel-mediated currents underlie high-fat diet induced vagal afferent dysfunction. *Am J Physiol Gastrointest Liver Physiol*. 2018;315(4):G592–G601.
28. Zhao H, Simasko SM. Role of transient receptor potential channels in cholecystokinin-induced activation of cultured vagal afferent neurons. *Endocrinology*. 2010;151(11):5237–5246.
29. Grisanti LA, Kurada L, Cilz NI, Porter JE, Lei S. Phospholipase C not protein kinase C is required for the activation of TRPC5 channels by cholecystokinin. *Eur J Pharmacol*. 2012;689(1-3):17–24.
30. Lee JH, Kim SY, Kwon YK, Kim BJ, So I. Characteristics of the cholecystokinin-induced depolarization of pacemaking activity in cultured interstitial cells of Cajal from murine small intestine. *Cell Physiol Biochem*. 2013;31(4-5):542–554.
31. Burdakov D, Ashcroft FM. Cholecystokinin tunes firing of an electrically distinct subset of arcuate nucleus neurons by activating A-Type potassium channels. *J Neurosci*. 2002;22(15):6380–6387.
32. Cascio MG, Valeri D, Tucker SJ, Marini P. A1-adenosine acute withdrawal response and cholecystokinin-8 induced contractures are regulated by Ca(2+)- and ATP-activated K(+) channels. *Pharmacol Res*. 2015;95-96:82–91.
33. Maton PN, Selden AC, Chadwick VS. Differential distribution of molecular forms of cholecystokinin in human and porcine small intestinal mucosa. *Regul Pept*. 1984;8(1):9–19.

34. Oh EJ, Weinreich D. Bradykinin decreases K(+) and increases Cl(-) conductances in vagal afferent neurones of the guinea pig. *J Physiol (Lond)*. 2004;558(Pt 2):513–526.
35. Ozaki T, Mohammad S, Morioka E, Takiguchi S, Ikeda M. Infant satiety depends on transient expression of cholecystokinin-1 receptors on ependymal cells lining the third ventricle in mice. *J Physiol (Lond)*. 2013;591(5):1295–1312.
36. Kinch DC, Peters JH, Simasko SM. Comparative pharmacology of cholecystokinin induced activation of cultured vagal afferent neurons from rats and mice. *PLoS ONE*. 2012;7(4):e34755.
37. Ni YL, Kuan AS, Chen TY. Activation and inhibition of TMEM16A calcium-activated chloride channels. *PLoS ONE*. 2014;9(1):e86734.
38. Pifferi S, Cenedese V, Menini A. Anoctamin 2/TMEM16B: a calcium-activated chloride channel in olfactory transduction. *Exp Physiol*. 2012;97(2):193–199.
39. Scudieri P, Sondo E, Caci E, Ravazzolo R, Galietta LJ. TMEM16A-TMEM16B chimaeras to investigate the structure-function relationship of calcium-activated chloride channels. *Biochem J*. 2013;452(3):443–455.
40. Bradley E, et al. Pharmacological characterization of TMEM16A currents. *Channels (Austin)*. 2014;8(4):308–320.
41. Pifferi S, Dibattista M, Menini A. TMEM16B induces chloride currents activated by calcium in mammalian cells. *Pflugers Arch*. 2009;458(6):1023–1038.
42. Swartz TD, Savastano DM, Covasa M. Reduced sensitivity to cholecystokinin in male rats fed a high-fat diet is reversible. *J Nutr*. 2010;140(9):1698–1703.
43. French SJ, Murray B, Rumsey RD, Sepple CP, Read NW. Preliminary studies on the gastrointestinal responses to fatty meals in obese people. *Int J Obes Relat Metab Disord*. 1993;17(5):295–300.
44. Wang R, et al. The volume-regulated anion channel (LRRC8) in nodose neurons is sensitive to acidic pH. *JCI Insight*. 2017;2(5):e90632.
45. Raybould HE, Taché Y. Cholecystokinin inhibits gastric motility and emptying via a capsaicin-sensitive vagal pathway in rats. *Am J Physiol*. 1988;255(2 Pt 1):G242–G246.
46. Grundy S. Toward optimal health: Scott Grundy, M.D., Ph.D. discusses metabolic syndrome (interviewed by Jodi R. Godfrey). *J Womens Health (Larchmt)*. 2005;14(10):883–888.
47. Krieger JP, et al. Glucagon-like peptide-1 regulates brown adipose tissue thermogenesis via the gut-brain axis in rats. *Am J Physiol Regul Integr Comp Physiol*. 2018;315(4):R708–R720.
48. Blouet C, Schwartz GJ. Duodenal lipid sensing activates vagal afferents to regulate non-shivering brown fat thermogenesis in rats. *PLoS ONE*. 2012;7(12):e51898.
49. Madden CJ, Santos da Conceicao EP, Morrison SF. Vagal afferent activation decreases brown adipose tissue (BAT) sympathetic nerve activity and BAT thermogenesis. *Temperature (Austin)*. 2017;4(1):89–96.
50. Madden CJ, Morrison SF. A high-fat diet impairs cooling-evoked brown adipose tissue activation via a vagal afferent mechanism. *Am J Physiol Endocrinol Metab*. 2016;311(2):E287–E292.
51. Williams EK, Chang RB, Strochlic DE, Umans BD, Lowell BB, Liberles SD. Sensory Neurons that Detect Stretch and Nutrients in the Digestive System. *Cell*. 2016;166(1):209–221.
52. Liddle RA, Goldfine ID, Rosen MS, Taplitz RA, Williams JA. Cholecystokinin bioactivity in human plasma. Molecular forms, responses to feeding, and relationship to gallbladder contraction. *J Clin Invest*. 1985;75(4):1144–1152.
53. Smith GP, Gibbs J, Jerome C, Pi-Sunyer FX, Kissileff HR, Thornton J. The satiety effect of cholecystokinin: a progress report. *Peptides*. 1981;2 Suppl 2:57–59.
54. Raybould HE, et al. Detection of macronutrients in the intestinal wall. *Auton Neurosci*. 2006;125(1-2):28–33.
55. Tsujino N, et al. Cholecystokinin activates orexin/hypocretin neurons through the cholecystokinin A receptor. *J Neurosci*. 2005;25(32):7459–7469.
56. Yamanaka A, Sakurai T, Katsumoto T, Yanagisawa M, Goto K. Chronic intracerebroventricular administration of orexin-A to rats increases food intake in daytime, but has no effect on body weight. *Brain Res*. 1999;849(1-2):248–252.
57. Nakamura T, et al. Orexin-induced hyperlocomotion and stereotypy are mediated by the dopaminergic system. *Brain Res*. 2000;873(1):181–187.
58. Hara J, et al. Genetic ablation of orexin neurons in mice results in narcolepsy, hypophagia, and obesity. *Neuron*. 2001;30(2):345–354.
59. Gibbs J, Falasco JD, McHugh PR. Cholecystokinin-decreased food intake in rhesus monkeys. *Am J Physiol*. 1976;230(1):15–18.
60. Kopin AS, et al. The cholecystokinin-A receptor mediates inhibition of food intake yet is not essential for the maintenance of body weight. *J Clin Invest*. 1999;103(3):383–391.
61. Schick RR, Yaksh TL, Go VL. Intracerebroventricular injections of cholecystokinin octapeptide suppress feeding in rats--pharmacological characterization of this action. *Regul Pept*. 1986;14(4):277–291.
62. Hirosue Y, et al. Effects of CCK antagonists on CCK-induced suppression of locomotor activity in mice. *Peptides*. 1992;13(1):155–157.
63. Marty A, Tan YP, Trautmann A. Three types of calcium-dependent channel in rat lacrimal glands. *J Physiol (Lond)*. 1984;357:293–325.
64. Mercer SW, Trayhurn P. Effect of high fat diets on the thermogenic activity of brown adipose tissue in cold-acclimated mice. *J Nutr*. 1984;114(6):1151–1158.
65. Cypess AM, et al. Identification and importance of brown adipose tissue in adult humans. *N Engl J Med*. 2009;360(15):1509–1517.
66. van Marken Lichtenbelt WD, et al. Cold-activated brown adipose tissue in healthy men. *N Engl J Med*. 2009;360(15):1500–1508.
67. Liu C, et al. PPARγ in vagal neurons regulates high-fat diet induced thermogenesis. *Cell Metab*. 2014;19(4):722–730.
68. Ritter RC, Brenner LA, Tamura CS. Endogenous CCK and the peripheral neural substrates of intestinal satiety. *Ann N Y Acad Sci*. 1994;713:255–267.
69. Duplus E, Glorian M, Forest C. Fatty acid regulation of gene transcription. *J Biol Chem*. 2000;275(40):30749–30752.
70. Lu Y, Whiteis CA, Sluka KA, Chapleau MW, Abboud FM. Responses of glomus cells to hypoxia and acidosis are uncoupled, reciprocal and linked to ASIC3 expression: selectivity of chemosensory transduction. *J Physiol (Lond)*. 2013;591(4):919–932.
71. Grynkiewicz G, Poenie M, Tsien RY. A new generation of Ca2+ indicators with greatly improved fluorescence properties. *J Biol Chem*. 1985;260(6):3440–3450.

72. Lu Y, et al. The ion channel ASIC2 is required for baroreceptor and autonomic control of the circulation. *Neuron*. 2009;64(6):885–897.
73. Sun H, Xia Y, Paudel O, Yang XR, Sham JS. Chronic hypoxia-induced upregulation of Ca2+-activated Cl- channel in pulmonary arterial myocytes: a mechanism contributing to enhanced vasoreactivity. *J Physiol (Lond)*. 2012;590(15):3507–3521.
74. Dutta AK, et al. Identification and functional characterization of TMEM16A, a Ca2+-activated Cl- channel activated by extracellular nucleotides, in biliary epithelium. *J Biol Chem*. 2011;286(1):766–776.
75. Davis AJ, et al. Potent vasorelaxant activity of the TMEM16A inhibitor T16A(inh) -A01. *Br J Pharmacol*. 2013;168(3):773–784.
76. Twyffels L, et al. Anoctamin-1/TMEM16A is the major apical iodide channel of the thyrocyte. *Am J Physiol, Cell Physiol*. 2014;307(12):C1102–C1112.
77. Maurya DK, Menini A. Developmental expression of the calcium-activated chloride channels TMEM16A and TMEM16B in the mouse olfactory epithelium. *Dev Neurobiol*. 2014;74(7):657–675.
78. Talaga AK, Dong FN, Reisert J, Zhao H. Cilia- and Flagella-Associated Protein 69 Regulates Olfactory Transduction Kinetics in Mice. *J Neurosci*. 2017;37(23):5699–5710.
79. Zeng X, et al. TMEM16A regulates portal vein smooth muscle cell proliferation in portal hypertension. *Exp Ther Med*. 2018;15(1):1062–1068.
80. Dibattista M, et al. Calcium-activated chloride channels in the apical region of mouse vomeronasal sensory neurons. *J Gen Physiol*. 2012;140(1):3–15.
81. Billig GM, Pál B, Fidzinski P, Jentsch TJ. Ca2+-activated Cl− currents are dispensable for olfaction. *Nat Neurosci*. 2011;14(6):763–769.
82. Nassar MA, et al. Nociceptor-specific gene deletion reveals a major role for Nav1.7 (PN1) in acute and inflammatory pain. *Proc Natl Acad Sci USA*. 2004;101(34):12706–12711.
83. Gautron L, Sakata I, Udit S, Zigman JM, Wood JN, Elmquist JK. Genetic tracing of Nav1.8-expressing vagal afferents in the mouse. *J Comp Neurol*. 2011;519(15):3085–3101.
84. Weidemann BJ, et al. Dietary Sodium Suppresses Digestive Efficiency via the Renin-Angiotensin System. *Sci Rep*. 2015;5:11123.
85. Maeda N, et al. Diet-induced insulin resistance in mice lacking adiponectin/ACRP30. *Nat Med*. 2002;8(7):731–737.